Research Journal of Recent Sciences _____ ISSN 2277-2502
Vol. **1 (ISC-2011),** 202-206 **(2012)** *Res.J.Recent Sci.*

Synthesis, Characterization and Hydrophilic Properties of Nanocrystalline $ZnFe_2O_4$ Oxide

Bangale Sachin and Bamane Sambaji
Department of Chemistry, Dr. Patangrao Kadam Mahavidyalaya, Sangli, MS, India

Available online at, www.isca.in
(Received 10th September 2011, revised 16th January 2012, accepted 28th January 2012)

Abstract

This study reports on synthesis of nano sized mixed oxides $ZnFe_2O_4$ was prepared by novel self combustion method using urea as a fuel. The processing features and the micro structural characteristics of $ZnFe_2O_4$ phases formed during self combustion reaction of the gels have been investigated by TG-DTA, SEM, XRD, and EDX and TEM. It has been found that the nanoscale composite powders of $ZnFe_2O_4$, directly obtained through the in situ self combustion reactions within the gel are composed of loosely agglomerated particles with sizes of ~100 nm, while these particles themselves are the aggregates of finer $ZnFe_2O_4$ and crystallites of 22- 32 nm in size. The densities of sintered oxides evaluated by different methods are a,roximately same. The superhydrophilicity of the sintered oxides was investigated by wetting experiments, by the sessile drop technique, were carried out at room temperature in air to determine the surface and interfacial interactions.

Keywords: XRD, combustion method, nanomaterial, $znfe_2o_4$.

Introduction

Recently, nanostructures like nanowires, nanobelts and nanodiskettes, have gained a considerable attention due to their potential in the development of smart functional materials, devices and system[1]. Sensors for biotechnological, industrial, environmental, food pharmaceutical, medical and related a, lications. Optical sensors for oxygen have been used for noninvasive analysis of dissolved oxygen in shake flasks for cell cultures. The oxygen sensitive element is a thin, luminescent patch affixed to the inside bottom of the flask. Both intensity and decay time may be measured[2,3]. Unlike, optical and electrochemical sensors. Solid state gas sensors based on semiconductors metal oxides may be a promising alternative, since them after good sensors properties and can be easily mass produced. Several semiconducting metal oxide viz. La-doped SnO_2[4,5], $BaTiO_3$.

It is well known that the semiconducting oxides such as ZnO, SnO_2, Fe_2O_3, Ga_2O_3, Sb_2O_3[6.7]. Are sensitive to toxic and inflammable gases. Among the chemical sensors $LaCoO_3$, $BaTiO_3$, $LaFeO_3$, $LaMnO_3$ etc. are perovskite-type materials of general formula ABO_3 are extensively studied owing to their notable gas sensitivity for different poisonous gases in addition to their magnetic, catalytic and other physical properties. The perovskite-type metal oxide including the d-block and rare earth elements has attracted the attention of many researchers due to their homogeneity, interesting structural, catalytic and gas sensing properties. There is an increasing interest in finding new materials in order to develop high performance solid state gas sensors. Gas sensors are important in environmental monitoring home safety and chemical controlling. Many different semiconducting oxides in bulk ceramic[8.9], thick film[10] and thin film[11.12]. Form have been studied as a candidate sensor element for gas sensing, spinel-type oxide semiconductors (ferrites) are an alternative for inexpensive and robust detection system because of good chemical and thermal stability under operating conduction. The sensing mechanism consists in the change of electrical resistivity resulting from chemicals reaction between gas molecules and the metal oxide surface[13,14]. The surface morphology has an essential role on the sensitivity of solid-state sensors. The nanograined materials offer new o,ortunities for enhancing the performance of gas sensors because of their high surface to volume ratio[15,16]. Several studies have reported that by finely controlling the micro/nanostructure or chemical composition of a surface, the adhesion between the superhydrophobic surface and water can be changed. Such superhydrophobic sur-faces show potential in a variety of a,lications from antisticking, anticontamination and self cleaning to anticorrosion and low friction coatings and gas sensing[17-20].

In this paper a sol-gel self combustion method was a,lied to prepare nanostructured zinc ferrites. The rapid heating and cooling during self combustion reaction can produce materials with high specific surface area which is beneficial for Hydrophilic test.

Material and Methods

In this study, $ZnFe_2O_4$ powder was synthesized by solution combustion technique using the starting regents as $Zn(NO_3)_26H_2O$ (7.43g), Fe $(NO_3)_26H_2O$ (7.27g) and urea (6.05g) as a fuel. urea possesses a high heat of combustion. It is an organic fuel providing a platform for redox reactions

during the course of combustion. Initially the zinc nitrates, iron nitrates and urea are taken in the 1,1,4 stoichiometric amount and homogenous paste was made. The paste formed was evaporated on hot plate in temperature range of 70 to 80^0C to result into a thick gel. The gel was kept on a hot plate for auto combustion and heated in the temperature range of 170 to 180^0C. The nanocrystalline $ZnFe_2O_4$ powder was formed within five minutes. The powder was sintered at 300, 500, 800, and 1000^0C for 4 hr. which resulted in to a brown color shining powder.

Results and Discussion

TG-DTA analysis: TG-DTA analysis was performed at a heating rate of 10 K min^{-1} to investigate the thermal properties of. $ZnFe_2O_4$. The TG spectrum and its 1st derivative in figure-1 show the thermal decomposition of $ZnFe_2O_4$ is the curve indicates that the slight weight loss in $ZnFe_2O_4$ powder due to little loss about 14.66 at temperature up to 200^0C in $ZnFe_2O_4$ of moisture, carbon dioxide and nitrogen gas. The DTA curve of $ZnFe_2O_4$ recorded in static air and in shown in figure-1.

The curve shown that $ZnFe_2O_4$ did not decompose, but weight loss was due to dehydrogenation, decarboxylation and denitration. Further weight loss of about 16% between the temperature range 400^0C and continuous loss in weight about 33.33% up to 550^0C is attributed to loss of organic materials and yield final product at 600^0C, this weight loss and weight gained was very negligible. This weight change was in the range of 800^0C these indicating that the synthesized powder was almost stable from the begging. The formation temperature in the present work is found to be comparatively similar than that reported for corresponding solid state reaction route.

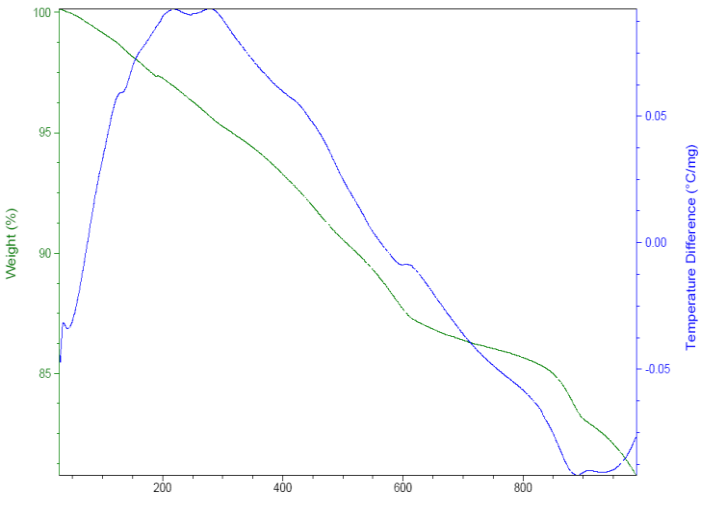

Figure-1
DTA-TG the prepared $ZnFe_2O_4$ nominal composition

X-ray Diffraction analysis: The X-ray diffraction pattern of $ZnFe_2O_4$ powder is shown in figure- 2. The observed d values compared with standard d values and are in good agreement with standard d value JCPDS data card number 82-1042. The structure possesses the cubic may be attributed to the different preparation method which may yield different structural defects. The crystalline size was determined from full width of half maximum (FWHM) of the most intense peak obtained by shown scanning of X-ray diffraction pattern. The grain size was calculated by using Scherrer's formula: $d = 0.9\lambda/ \beta\cos\theta$

The crystalline size can be calculated by using Scherrer equation[21,22]. Where, d is the crystalline size, λ is the X-ray wavelength of the Cu K_α source (λ=1.54056 A^0), β is the FWHM of the most predominant peak at 100 % intensity, θ is the Braggs angle at which peak is recorded. In order to obtain pure nanocrystalline $ZnFe_2O_4$ particles and understand the thermal characterizations, the as prepared $ZnFe_2O_4$ powder is further calcined at 180, 300, 500, 800 and 1000^0C respectively (the calcined temperature assigned as T_C). Figure-2 present XRD patterns for $ZnFe_2O_4$ oxide nanoparticles. The effects of the calcinations temperature on the crystallite size of $ZnFe_2O_4$ particles can be demonstrated. Traces of $ZnFe_2O_4$ crystallites phases (111), (311), (400), (422) and (511) are detected in the XRD pattern for all calcined temperatures and then their intensities increase abruptly when the T_C above 1000^0C. In general, the sharpness of the XRD peak (i.e. high crystallinity) is increased as the T_C increases.

According to the (311) diffraction pattern of $ZnFe_2O_4$ crystalline, the particle size of $ZnFe_2O_4$ can be calculated from the full width at haif-maximum using the Scherrer equation. Obviously, the particle size of $ZnFe_2O4$ changes as the *Tc* controlled fewer than 180, 300, 500, 800 and 1000^0C, the order is 22, 22, 25, 32 and 32 nm, respectively. These indicate that the crystallinity of $ZnFe_2O_4$ is accelerated as the *Tc* above 500^0C. Illustrates the relationship between the annealing temperature and the average crystal size of the $ZnFe_2O_4$ nanoparticles. It is obvious that the $ZnFe_2O_4$ nanoparticle grows slowly at 300-500^0C and 800-1000^0C, respectively, the nanoparticle grow rapidly at 800^0C.

Particle size Analyzer: Particle size distribution studies Figure-3 have been carried out by using dynamic light scattering techniques (DLS) *via* laser input energy of 632 nm).

It was observed that zinc cobalt oxide nanoparticles particles have narrow size distribute within the range of about 30-40 nm. Which well matches are with calculated from Debye-Scherrer equation.

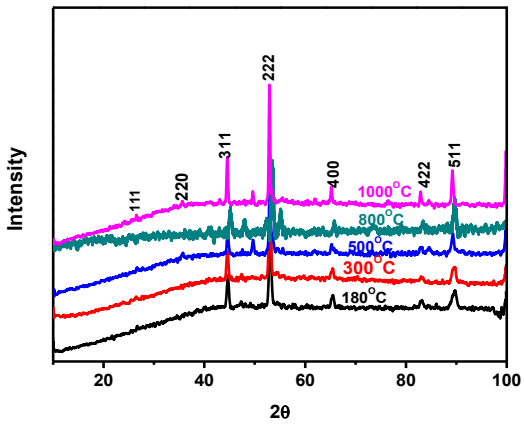

Figure-2
XRD patterns for $ZnFe_2O_4$ oxide nanoparticales 180, 300, 500, 800 and 1000^{0}C

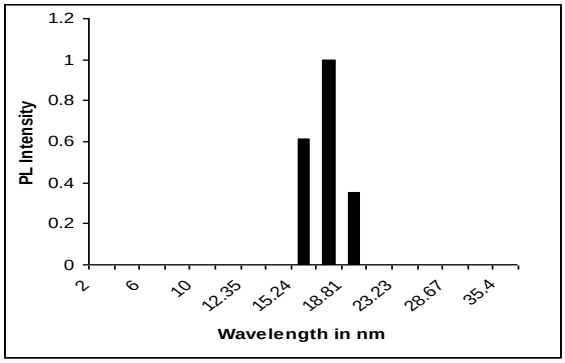

Figure-3
Particle Size Distribution of $ZnFe_2O_4$ oxide Nanoparticale

Scanning electron micrograph analysis: The microstructure of the sintered samples can be visualized from scanning electron microscope (SEM) tool. Figure- 4 shown the particle morphology of high resolution, the particle are most irregular in shape with a Nanosize range. Some particles are found as agglomerations containing very fine particles the particles shapes are not defined porous nature and small and large core, spongy pores are seen in the micrograph.

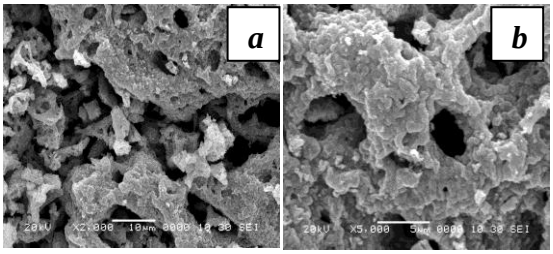

Figure-4
SEM images of the self combustion product the powder annealed at 800^{0}C at (a) and (b) high resolution

Energy dispersive X-ray microanalysis analysis (EDX), Figure-4 shows the energy dispersive X-ray spectrum of $ZnFe_2O_4$. This was carried out to understand the composition of zinc, iron and oxygen in the material. There was no unidentified peak observed in EDX. This confirms the purity and the composition of the $ZnFe_2O_4$ nanomaterial

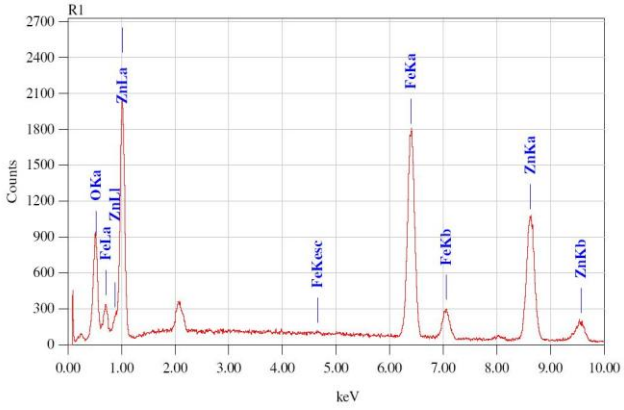

Figure-5
EDX pattern of $ZnFe_2O_4$

Transmission electron microscopy analysis (TEM), The TEM image of the mixed precursor calcined at 800^{0}C for 2h are shown in figure- 6. It indicates the presence of $ZnFe_2O_4$ nanoparticles with size 30-40 nm which form beed type of oriental aggregation throughout the region. The HRTM image figure- 6 (b) shows well developed lattice fringes, which are correlated well with the XRD result. The selected area electron diffraction (SAED) pattern figure- 6 (a) shows the spot type pattern which is indicative of the presence of single crystalline particles. No evidence was found for more than one pattern, suggesting the single phage nature of the material.

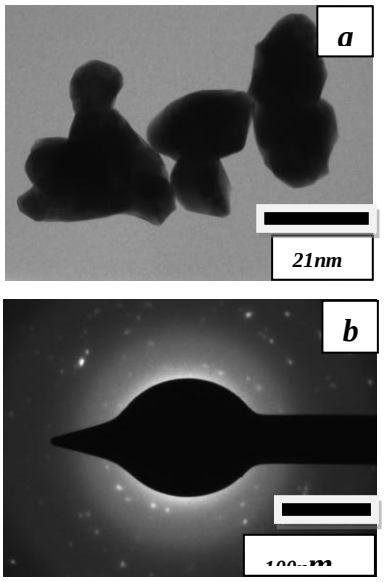

Figure-6
TEM image of the combustion product after annealing at 800^{0}C for .and HRTEM image of the same (b) with the inset showing the SAED pattern on the spot in (a)

Density measurement: Density evaluation from X-ray data, The X-ray density of the samples has been computed from the values of lattice parameters using the formula [23-24]. $d = 8M/Na^3$, Where 8 represent the number of molecules in a unit cell of a spinel lattice, M the molecular weight of the sample, N the Avogadro's number, and a the lattice parameter of the sample. The lattice constant for the cubic was calculated using the equation $d = a/ (h^2+k^2+l^2)^{1/2}$.

Tap density: The as prepared $ZnFe_2O_4$ was crushed in an agate mortar using a pestle and a mortar. A known amount of this powder was filled into a graduated cylinder of 10 ml capacity. The cylinder was ta,ed until the powder level remained unchanged. The volume occupied by the powder was noted. The ratio between the weight of the substance and the volume gave tap density[25].

Powder density: The powder densities were measured using Archimedes principal [26] with a picometer and xylene as a liquid medium. The pynometer of volume 10 ml was used. The following weight were taken and used in the density calculation.
Weight of the bottle + W_{1g}, Weight of the bottle + substance = W_{2g},
Weight of the bottle + substance + xylene =W_{3g},
Weight of the bottle + xylene + W_{4g},
Density of xylene = ρ_{sol}. $\rho=(W_2-W_1)\ \rho_{sol}/(W_4-W_3) + (W_2-W_1)$

Table-1
Densities of $ZnFe_2O_4$ in kg/m^3

Sample	Density from XRD	Tap density	Bulk density
$ZnFeO_4$	6170.22	6188.12	6138.888

Superhydrophilic Test : Wettability shows the behavior of water droplet on u,er surface of material depends on surface energy and surface roughness of material. Thomas Young had described the force acting on a liquid droplet spreading on surface. The so-called contact angle (θ) is related to interfacial energies acting between the solid-liquid (γ_{SL}), solid-vapor (γ_{SV}) and liquid-vapor (γ_{LV}) given by relation.

$$\cos\theta = \frac{(\gamma_{SV} - \gamma_{SL})}{\gamma_{LV}} \qquad (1)$$

The expression given by Equation 1 is strictly valid only for surfaces that are atomically smooth, chemically homogeneous, and those that do not change their characteristics due to interactions of the probing liquid with the substratum, or any other outside force. Wenzel regime, the liquid wets the surface, but the measured contact angle (θ*) differs from the "true" contact angle (θ) by Wenzel's equation for rough surface r > 1 [27.-30].

$$\cos\theta^* = r\cos\theta \qquad (2)$$

Where r is the roughness factor of the surface. The wettability nature of our synthesized material is super hydrophilic in the Wenzel because of highly rough surface nature clearly seen from SEM images with consideration given to the surface roughness.Figure-5 (a-b) shows the image of contact angle on rough surface of zinc iron oxide material. It seen that contact angle of material is θ =0, hence material in superhydrophilic ((θ ≤ 5) may be due to high energy surface and porous nature.

In to characterization: Wetting experiment of synthesized pure zinc iron oxide evaluated by contact angle measurement were performed by the sessile drop method using an Advanced goniometer (Model110, Ram hart Instrument Co., USA) a,aratus and distilled water droplets (0.01ml) were delivered to surface of zinc iron oxide material at different points.

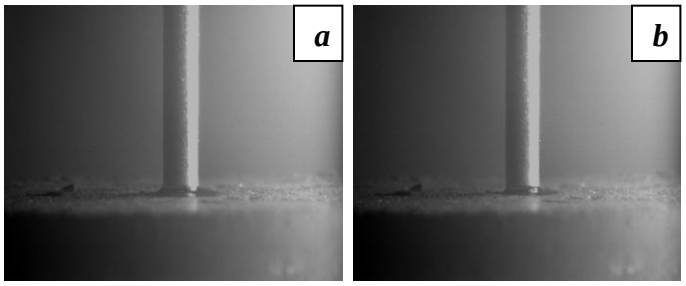

Figure-7 (a-b)
Photograph of measured contact angle on rough surface of zinc iron oxide materials.

Conclusion

Nanocrystalline $ZnFe_2O_4$ has been synthesized by self combustion route. This synthesis route may be used for the synthesis of other metal oxide, characterization by using SEM micrographs show a porous structure and submicron grains 100 nm, by XRD technique the average crystal size of the $ZnFe_2O_4$ nanoparticles ranges from about 22, 22, 25, 32 and 32 nm. under 180-1000^{0}C. Elemental analysis confirmed by using EDX. Density can be carried out by different technique it was found to a,roximately same. Wetability of this material obtained from contact angle goniometer. The contact angle (θ) is zero, which indicates that oxide material was superhydrophilic.

Acknowledgment

The S.V.Bangale are grateful to the Principal, Dr. Patangrao Kadam Mahavidyalaya, Sangli India for providing laboratory facilities and authors thankful for to Mr. Satish A. Mahadik for help in hydrophilic studies.

References

1. Martinelli G., Carotta Cristina M., Ferroni M., Sadaoka Y. and Traversa E., *Sens. Actuators* B Chem **55**, 99-110 **(1999)**

2. Tolosa L., Kostov Y., Harms P. and Rao *G., Biotechnol, Bioeng* **80 (5),** 594-597 **(2002)**

3. Wittmann C., Kim M.H. and Heinzle J.C., *E. Biotechnol Litt*., **25 (5),** 377-380 **(2003)**

4. Kim D.H., Yoon J.Y., Park C.H. and Kim K.H., CO_2 sensing characteristics of SnO_2 thick film by coating Lanthanum oxide, *Sens. Actuators* B, **26,** 61-66 **(2000)**

5. Marsal A., Cornet A. and Morante R.J., study of the CO and humidity interference in La doped tin oxide CO_2 gas sensors, *Sens. Actuators*, B, **94** , 324-329 **(2003)**

6. Ishihara T., Kometani K. and Takita Y., Improved sensitivity of CuO-$BaTiO_3$ capacitive-type CO_2 sensors by additives, *Sens. Actuators* B**, 28**, 49-54 **(1995)**

7. Lee M.S. and Meyer J.U., A new process for fabricating CO2 sensing layers based on $BaTiO_3$ and additives. *Sens. Actuators* B**, 68**, 293-299 **(2000)**

8. Moseley P.T., solid state gas sensors, *Metas. Sci Technol*, **8,** 223-237 **(1997)**

9. Srivastava R. and Dwivedi R. and Srivastava S.K., Development of high sensitivity tin oxide based sensors for gas/odor detection at room temperature, *Sens.Actuators* B, **50**, 175-180 **(1998)**

10. Tianshu Z., Ruifang Z., Yusheng S. and Xinggin L., Influence of Sb/Fe ratio and heating temperature on microstructure and gas sensing property of Sb_2O_3-Fe_2O_3 complex oxide semi-conductors, *Sens.Actuators* B, **32,** 185-189 **(1996)**

11. Comini E., Ferroni M, Guidi V., Fagila G, Martinelli G. and Sberverglieri G., Nanostructured mixed oxide compounds for gas sensing a,lication, *Sens. Actuators B, Chem*., **84**, 26-32 **(2002)**

12. Rezlescu N., Doroftei C., Rezlescu E. and Popa P.D., The influence of Sn4+ and /Mo6+ ions on the structure, electrical and gas sensing properties of Mg-Ferrite *Phys.Stat solid* A **203**, 306-316 **(2006)**

13. Patil D.R., Patil L.A., Jain G.H., Wagh M.S. and Patil S.A., Surface activated ZnO thick film resistors for LPG gas sensing, *Sens.Transducers* J., **74**, 874-883 **(2006)**

14. Jin Z., ZhonH.J. and Jin Z.L., Savinell and Liu C.C., A,lication of nano-crystalline porous tin oxide thin film for CO sensing *Sens. Actuators* B, Chem. **15**, 188-194 **(1998)**

15. Ferreira I., Igreja R. ,.Fortunato R. and Martins R., porous a/hc-Si films produced by HW-CVD as ethanol vapour detector and primary fuel cell, *Sens. Actuators* B, Chem. **103**, 344-349 **(2004)**

16. Gurlo A., Barsan N. and Weimar U., mechanism of CO_2 sensing on SnO_2 and InO_3 thick film sensors as revealed by simultaneous consumption and resistivity measurements in the 16th European conference on Solid-state Transducers praque Czech, Republic **15-18** Sept, 970-933 **(2002)**

17. Maffeis T, G., Owen G.T. and Penny M.W., Starke T.K.H. Clark S.A., Ferkel H. Wilks S.P., Nano-crystalline SnO_2 gas sensors response to O_2 and CH_4 at elevated temperature investigated by XPS, *Surf. Sci*. **520**, 29-34 **(2002)**

18. Rella R., Siciliana P., Capone S., Epifani M., Vasanelli L., Liciulli A., Air quality monitoring by means of Sol-Gel integrated tin oxide thin film, *Sens.Actuators* B, Chem**. 58,** 283-288 **(1999)**

19. Martins R., Fortunato E., Nunes P.,Fereira I. and Marqunes A., Zinc oxide as ozone sensors *J. A,l. Phys.* **96**, 1398-1408 **(2004)**

20. Rezlescu N., Iftimie N., Reziescu E., Doroftei C. and Popa P.D., semiconducting gas sensors for acetone based on the grained nickel ferrite, *Sens. Actuators* B, Chem. **114**, 427-432 **(2006)**

21. Dhere S.L. and Latthe S.S., Ka,enstein C., Rao A.V., *J. A,l. Surf. Sci*. **256,** 3967 **(2010)**

22. Feng L., Li S., Li H., Zhai J., Song Y., Jiang L. and Zhu D. , *Angew. Chem. Int. Ed. Engl*, **41** , 1221**(2002)**

23. Latthe S.S., Hiroaki Imai, Ganesan V. and Rao A.V., *J. A,l. Surf. Sci*. **256** , 217 **(2009)**

24. Chang K.C., Chen Y.K. and Chen H., *Surf. Coat. Technol*. **202** , 3822 **(2008)**

25. Crambelli P., et al and Turco, *A,l. Catal.* B, **24**, 243 **(2000)**

26. Cullity B., Elements of X-ray diffraction Addison Weley, London, 99 **(1956)**

27. Smith J., Wijn H.P., Phillips N.N. and Gloeilampenjabricken Eindhoven Ferrites Holland 144A, **(1959)**

28. Venkataraman A., Hiremath A.V., Date K.S. and Kulkarni M.S. *Bull. Mater.Sci*.**24**, 101 **(2000)**

29. Kinsman S., Richardson T.H. and Peterson R.V. (New York, Academic Press) Systematic materials analysis Vol. **4**, **(2000)**

30. Klug P.H. and Alexander L. X-ray diffraction procedure (New-York, John Wily) **(1962)**